

PAPER • OPEN ACCESS

Delving into the anisotropic interlayer exchange in bilayer CrI_3

To cite this article: Srdjan Stavić *et al* 2024 *2D Mater.* 11 015020

View the [article online](#) for updates and enhancements.

You may also like

- [Emerging intrinsic magnetism in two-dimensional materials: theory and applications](#)
Songrui Wei, Xiaoqi Liao, Cong Wang et al.
- [Deep learning methods for Hamiltonian parameter estimation and magnetic domain image generation in twisted van der Waals magnets](#)
Woo Seok Lee, Taegeun Song and Kyoung-Min Kim
- [Insights on magnon topology and valley-polarization in 2D bilayer quantum magnets](#)
Doried Ghader



PAPER

Delving into the anisotropic interlayer exchange in bilayer CrI₃

OPEN ACCESS

Srdjan Stavric^{1,2,*} , Paolo Barone³  and Silvia Picozzi¹RECEIVED
25 July 2023REVISED
7 November 2023ACCEPTED FOR PUBLICATION
6 December 2023PUBLISHED
15 December 2023

Original Content from
this work may be used
under the terms of the
[Creative Commons
Attribution 4.0 licence](#).

Any further distribution
of this work must
maintain attribution to
the author(s) and the title
of the work, journal
citation and DOI.

¹ Consiglio Nazionale delle Ricerche CNR-SPIN, c/o Università degli Studi 'G. D'Annunzio', 66100 Chieti, Italy² Vinča Institute of Nuclear Sciences—National Institute of the Republic of Serbia, University of Belgrade, PO Box 522, RS-11001 Belgrade, Serbia³ Consiglio Nazionale delle Ricerche CNR-SPIN, Area della Ricerca di Tor Vergata, Via del Fosso del Cavaliere, 100, I-00133 Rome, Italy

* Author to whom any correspondence should be addressed.

E-mail: srdjan.stavric@spin.cnr.it**Keywords:** bilayer CrI₃, interlayer Dzyaloshinskii–Moriya interaction, interlayer Kitaev interactionSupplementary material for this article is available [online](#)**Abstract**

Bilayer CrI₃ attracted much attention due to stacking-induced switching between the layered ferromagnetic and antiferromagnetic order. This discovery brought under the spotlight the interlayer Cr–Cr exchange interaction, which despite being much weaker than the intralayer exchange, plays an important role in shaping the magnetic properties of bilayer CrI₃. In this work we delve into the anisotropic part of the interlayer exchange with the aim to separate the contributions from the Dzyaloshinskii–Moriya (DMI) and the Kitaev interactions (KI). We leverage the density functional theory calculations with spin Hamiltonian modeling and develop an energy mapping procedure to assess these anisotropic interactions with μeV accuracy. After inspecting the rhombohedral and monoclinic stacking sequences of bilayer CrI₃, we reveal a considerable DMI and a weak interlayer KI between the sublattices of a monoclinic bilayer. We explain the dependence of DMI and KI on the interlayer distance, stacking sequence, and the spin–orbit coupling strength, and we suggest the dominant superexchange processes at play. In addition, we demonstrate that the single-ion anisotropy in bilayer CrI₃ is highly stacking-dependent, increasing by 50% from monoclinic to rhombohedral bilayer. Remarkably, our findings prove that iodines are highly efficient in mediating the DMI across the van der Waals gap, much owing to spatially extended $5p$ orbitals which feature strong spin–orbit coupling. Our study gives promise that the interlayer chiral control of spin textures, demonstrated in thin metallic films where the DMI is with a much longer range, can be achieved with similar efficiency in semiconducting two-dimensional van der Waals magnets.

1. Introduction

Since the long sought discovery of two-dimensional (2D) magnets finally happened with CrI₃ and Cr₂Ge₂Te₆ [1, 2], a large stream of scientific efforts has been directed towards achieving new capabilities with magnetic van der Waals (VdW) heterostructures [3–7]. Given the diversity of 2D materials, there is a profusion of possible magnetic VdW heterostructures that offer endless possibilities. Yet, to find intriguing phenomena, one does not need to look any further from the two layers of CrI₃. So far, the magnetic properties of bilayer CrI₃ have been manipulated by electric fields [8, 9], electrostatic doping [10], pressure

[11], and twisting [12]. In addition, theoretical studies proposed to switch the direction of magnetization in one of its two layers by spin-orbit torque [13] and predicted the magnetic photogalvanic effect [14], magnetic polarons [15], and magnetoelectric response in bilayer CrI₃ [16].

Monolayer CrI₃ is composed of chromium atoms arranged in a honeycomb lattice surrounded by edge-sharing iodine octahedra. Below the Curie temperature the $S = 3/2$ spins on Cr atoms are parallel and the monolayer CrI₃ is a ferromagnet (FM) with an out-of-plane magnetization [17–19]. The magnetic anisotropy energy (MAE), that is necessary for the long-range magnetic order to persist in 2D crystals at finite

temperatures [20], emerges in CrI_3 from an interplay between the single-ion anisotropy (SIA) and the two-ion anisotropy (TIA) occurring between the nearest neighbors Cr ions [17, 21]. The TIA is usually derived within the generalized Heisenberg–Kitaev model and gives rise, in addition to the conventional isotropic Heisenberg exchange, to the Kitaev exchange and to the symmetric pseudo-dipolar interaction, depending on the bond-orientation. These terms, which we will generally label as ‘Kitaev-like interaction’ (KI), refer to the traceless symmetric part of the most general expression for bilinear spin-spin interactions [22] and cooperate with dipole-dipole interaction in shaping the total magnetic anisotropy [23]. Like SIA, the KI in CrI_3 comes mostly from the spin–orbit coupling (SOC) on iodine atoms. MAE scales with the ligand SOC strength, being instrumental to CrI_3 showing a higher Curie temperature (T_C) than the isostructural CrBr_3 and CrCl_3 , whose ligands feature much weaker SOC than iodines [24–27]. Besides SIA and KI, SOC can give rise to the Dzyaloshinskii–Moriya interaction (DMI). However, the presence of an inversion center in the nearest neighbor Cr–Cr bonds imposes that this antisymmetric part of the anisotropic exchange is exactly zero. On the other hand, the DMI is allowed between the next-nearest Cr neighbors and, although tiny, it can play an important role in gapping the magnon spectra [28].

In addition to magnetic properties that bilayer CrI_3 inherits from its constitutive layers, the interlayer exchange has proven extremely important as it can affect the direction of layers’ magnetizations. It is an order of magnitude weaker than the intralayer exchange, but the possibility to tune it via stacking alternations made it a subject of numerous studies. For example, if we adopt the stacking from bulk CrI_3 that crystallizes either in rhombohedral (the low temperature or LT phase, $R\bar{3}$ space group) or monoclinic lattice (the high temperature or HT phase, $C/2m$ space group) [29], we end up with two different bilayer structures that we refer to as the LT and the HT structure (figures 1(a) and (b)). Here the theoretical [10, 30–33] and experimental [34] studies agree: the LT stacking favors the FM ordering of layers’ magnetizations, whereas the HT stacking leads to layered antiferromagnetic (AFM) order. However, being realized through (at least) two iodines, the interlayer Cr–Cr coupling is mostly of super-superexchange type, which makes its microscopic description complicated due to a high number of relevant hopping processes [35–37].

In bilayer CrI_3 studies galore the interlayer exchange is most often considered isotropic. This is a reasonable assumption for many purposes, given that the bilayer CrI_3 lattice is centrosymmetric and thus the DMI is forbidden, whereas the KI, if nonzero, is usually very small. However, the strict constraints imposed on DMI by the global symmetry of the structure do not forbid the DMI to appear locally, between

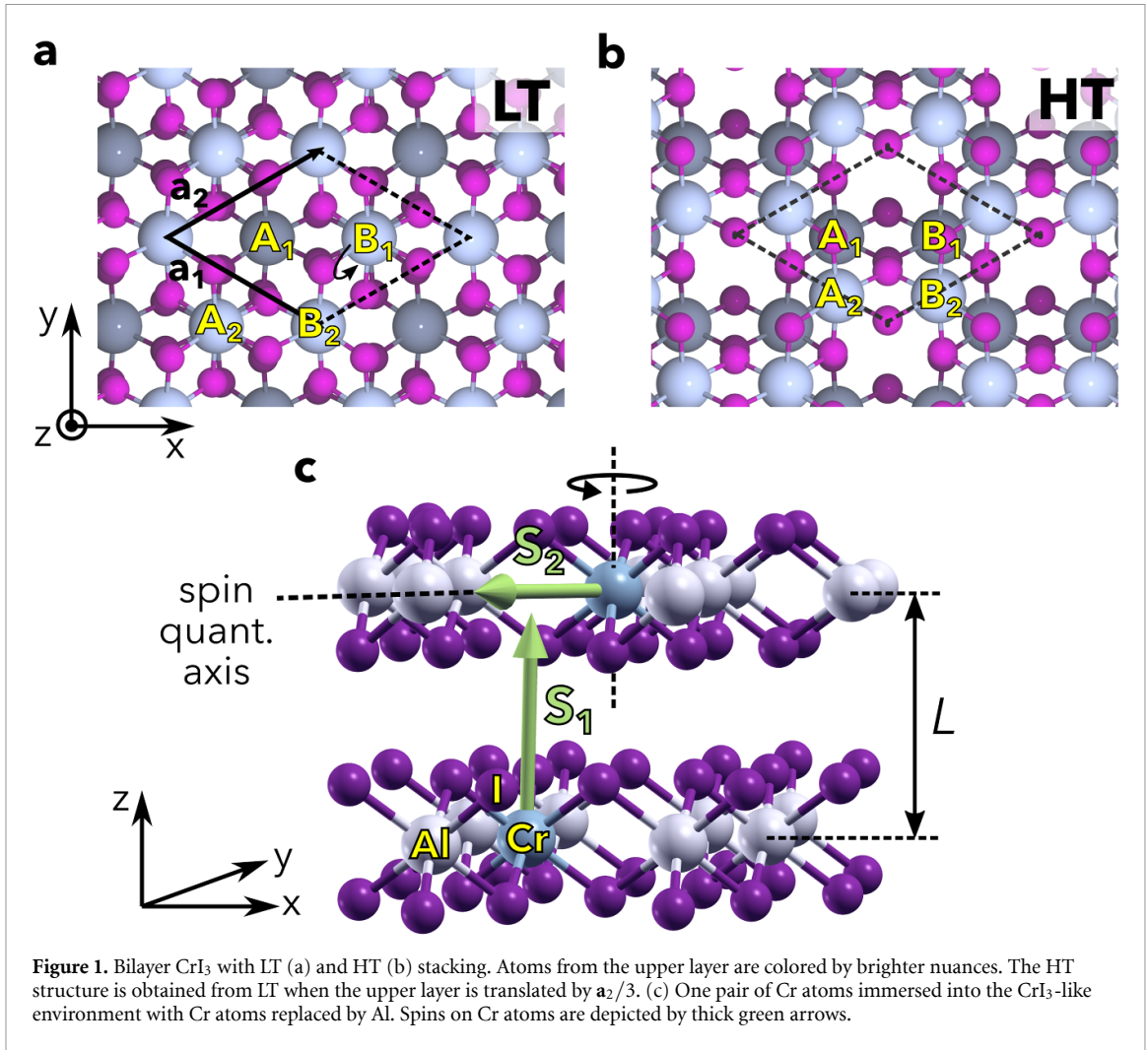
the specific neighbors. Moreover, if the DMI exists between the specific neighbors and the global symmetry constraints are somehow removed—the macroscopic DMI can emerge as well. New studies warm up such expectations showing that skyrmions—topologically protected particle-like spin textures that usually appear as a consequence of DMI—can be induced via moiré magnetic exchange interactions in twisted bilayer CrI_3 [12, 38, 39]. Concerning the interlayer DMI in general, Vedmedenko *et al* [40] proposed the atomistic model that predicts the formation of global chiral spin textures due to interlayer DMI between the ferromagnetic layers coupled through a nonmagnetic spacer. Recently, chiral control of spin textures is experimentally achieved in ferromagnetic TbFe/Pt/Co thin films, where the out-of-plane magnetization of TbFe is DMI-coupled with the in-plane magnetization of Co [41]. In this multilayer system the interlayer DMI is strong because the Pt atoms carry the conductive electrons that feature strong SOC. In analogy to TbFe/Pt/Co, the question is whether the iodine ligands, that also have considerable SOC, can play the role of DMI-mediator in bilayer CrI_3 . Moreover, having in mind the importance of KI in monolayer CrI_3 , how strong is the interlayer KI in bilayer CrI_3 ?

We present a theoretical study that combines the density functional theory (DFT) and Hamiltonian modeling in calculating the anisotropic part of the interlayer exchange in bilayer CrI_3 . The manuscript is organized as follows: we start by presenting the employed computational approach in section 2.1 and describe the model Hamiltonian that expresses the coupling between two perpendicular spins in section 2.2. The ability of the perpendicular-spins model to capture the changes in DFT band energies is demonstrated in section 2.3. The validity of the model is extended to describe the coupling between fully magnetized layers in section 2.4, where we reveal a considerable DMI and an order of magnitude weaker KI between the sublattices of bilayer CrI_3 . We demonstrate how both DMI and KI depend on structural transformations and the SOC strength in section 2.5, suggesting possible superexchange mechanisms governing these interactions. Finally, in section 3 we summarize the study by proposing a 2D magnetic heterostructure that should be a suitable platform for realizing the interlayer DMI coupling of layers’ magnetizations, similar to that experimentally achieved in thin metallic films.

2. Results

2.1. Computational approach

We model the bilayer CrI_3 by stacking two CrI_3 layers in rhombohedral (LT) and monoclinic (HT) sequences (figure 1). The structural details and computational parameters of DFT calculations are given in the section 4. In order to study the coupling



between the two spins from different layers, we need to isolate them from the rest of the magnetic environment. To solve this problem, we use the 2×2 supercell and replace by Al all the Cr atoms except the two whose interaction will be inspected (figure 1(c)). Al is trivalent like Cr, so the two remaining Cr atoms are embedded into the nonmagnetic crystalline environment reminiscent of that in bilayer CrI_3 . To check the validity of the atomic replacement method, we calculated the SIA and the intralayer nearest-neighbor exchange tensor \mathcal{J}_1 of monolayer CrI_3 and compared the results to those obtained with the reference four-state method [42] in supplementary information.

In calculating the interlayer exchange tensors, we follow a two-step computational procedure: in the first step the electron density and the Kohn–Sham wavefunctions are obtained from noncollinear self-consistent field calculations without SOC. The directions of spins \mathbf{S}_1 and \mathbf{S}_2 on Cr atoms are constrained perpendicular to one another (figure 1(c)) using the penalty functional [43]. In the second step the Kohn–Sham wavefunctions from the first step are used, the SOC is included and the sum of band energies is calculated for different directions of the spin quantization axis, which is rotated around a given axis. For

example, if \mathbf{S}_2 is parallel to the spin quantization axis, it will rotate together with it, whereas the direction of \mathbf{S}_1 is unaffected by rotation (see figure 1(c)). Given that only the sum of band energies is used, this procedure can be applied to any system provided that the use of the magnetic force theorem is justified [44–46]. This method can save more than 50% of the computational time (see the supplementary information for details) while offering the accuracy of the reference four-state method [42, 47].

2.2. Hamiltonian of two perpendicular spins

Here we derive the model describing the coupling of two perpendicular spins, that is used for mapping the differences between DFT band energies obtained for different directions of the spin quantization axis. In closer detail, we suppose that the two spins belong to different layers, but the model works as well if the spins are belonging to the same layer.

The total energy of such a two-spin system is

$$E = E_{\text{nm}} + \mathbf{S}_1 \mathcal{J} \mathbf{S}_2 + \mathbf{S}_1 \mathcal{A}_1 \mathbf{S}_1 + \mathbf{S}_2 \mathcal{A}_2 \mathbf{S}_2, \quad (1)$$

where E_{nm} is the nonmagnetic contribution, \mathcal{J} is an exchange tensor describing the interaction between

the spins \mathbf{S}_1 and \mathbf{S}_2 , and \mathcal{A}_i is the SIA tensor attributed to the spin \mathbf{S}_i . If the layers are structurally identical and magnetic atoms are Wyckoff partners sharing the same site symmetries, then $\mathcal{A}_1 = \mathcal{A}_2 = \mathcal{A}$. Without loss of generality, let us choose the coordinate system by fixing \mathbf{S}_1 along the z -axis and directing \mathbf{S}_2 in the xy -plane. Now, $\mathbf{S}_1 = (0, 0, S_1)$ and $\mathbf{S}_2 = (S_2 \cos(\phi), S_2 \sin(\phi), 0)$ and the spin configuration is completely determined by a single parameter—the angle ϕ between the \mathbf{S}_2 and the x -axis. The equation (1) turns into

$$\begin{aligned} E(\phi) &= E_C + S_1 S_2 (J_{zx} \cos(\phi) + J_{zy} \sin(\phi)) \\ &\quad + S_2^2 (A_- \sin^2(\phi) + A_+ \sin(2\phi)) \\ &= E_C + E_J(\phi) + E_A(\phi), \end{aligned} \quad (2)$$

where we introduced the parameters $A_- \equiv A_{yy} - A_{xx}$ and $A_+ \equiv (A_{xy} + A_{yx})/2$ for convenience and $E_C = E_{nm} + A_{zz} S_1^2 + A_{yy} S_2^2$ comprises all the ϕ -independent terms. The important terms for our discussion are the exchange interaction energy $E_J(\phi)$ and the contribution from the SIA $E_A(\phi)$. If we interchange the roles of \mathbf{S}_1 and \mathbf{S}_2 the equation (2) yields J_{xz} and J_{yz} . If we further change the rotation axis from z - to x -axis, J_{xy} and J_{yx} are obtained (and J_{xz} and J_{zx} that are known already). Therefore, by considering the sets of spin configurations that we denote as $\{\mathbf{S}_1 \parallel z \leftrightarrow \mathbf{S}_2 \circlearrowleft z\}$ and $\{\mathbf{S}_1 \parallel x \leftrightarrow \mathbf{S}_2 \circlearrowleft x\}$, one obtains all the off-diagonal \mathcal{J} -matrix elements.

In general, the \mathcal{J} tensor decomposes into the isotropic Heisenberg exchange and the anisotropic DMI (antisymmetric) and KI (symmetric) [47],

$$\begin{aligned} \mathcal{J} &= \underbrace{\frac{1}{3} \text{Tr}(\mathcal{J}) \mathbb{I}_3}_{\text{Heisenberg exchange}} + \underbrace{\frac{1}{2} (\mathcal{J} - \mathcal{J}^T)}_{\text{DMI}} \\ &\quad + \underbrace{\left[\frac{1}{2} (\mathcal{J} + \mathcal{J}^T) - \frac{1}{3} \text{Tr}(\mathcal{J}) \mathbb{I}_3 \right]}_{\text{anisotropic symmetric exchange (KI)}} \\ &= \frac{1}{3} \text{Tr}(\mathcal{J}) \mathbb{I}_3 + \mathcal{D} + \mathcal{K}. \end{aligned} \quad (3)$$

By assumption, the spins are perpendicular and the Heisenberg exchange between them vanishes. Thus, the exchange energy contains only the DMI and the KI contributions, $E_J(\phi) = E_{DM}(\phi) + E_K(\phi)$. The DMI is usually expressed as the mixed vector product, $E_{DM} = \mathbf{D} \cdot (\mathbf{S}_1 \times \mathbf{S}_2)$, which introduces the *Dzyaloshinskii vector*,

$$\mathbf{D} = (D_x, D_y, D_z) = \frac{1}{2} (J_{yz} - J_{zy}, J_{zx} - J_{xz}, J_{xy} - J_{yx}). \quad (4)$$

For a system with a well defined symmetry, the direction of \mathbf{D} can be (at least partially) determined with the help of Moriya rules [22]. In supplementary information we derive the Moriya rules in a form that is more suitable for our purposes.

Within $\{\mathbf{S}_1 \parallel z \leftrightarrow \mathbf{S}_2 \circlearrowleft z\}$ spin configurations, the total variation of the Kitaev energy is $\Delta E_K =$

$2S_1 S_2 (K_{zx}^2 + K_{zy}^2)^{1/2}$. In analogy to DMI, it is convenient to introduce the vector $\mathbf{K} = \frac{1}{2} (J_{yz} + J_{zy}, J_{zx} + J_{xz}, J_{xy} + J_{yx})$ that quantifies the strength of KI by $\Delta E_K / 2S_1 S_2 = (K_x^2 + K_y^2)^{1/2}$. In general, the matrix \mathcal{K} , unlike \mathcal{D} , contains the diagonal elements as well, that are out of reach of this method as their calculation requires the (anti)parallel spin configurations. Therefore, strictly speaking, for a given reference frame the parameter K quantifies the strength of the off-diagonal part of the Kitaev interaction (KI).

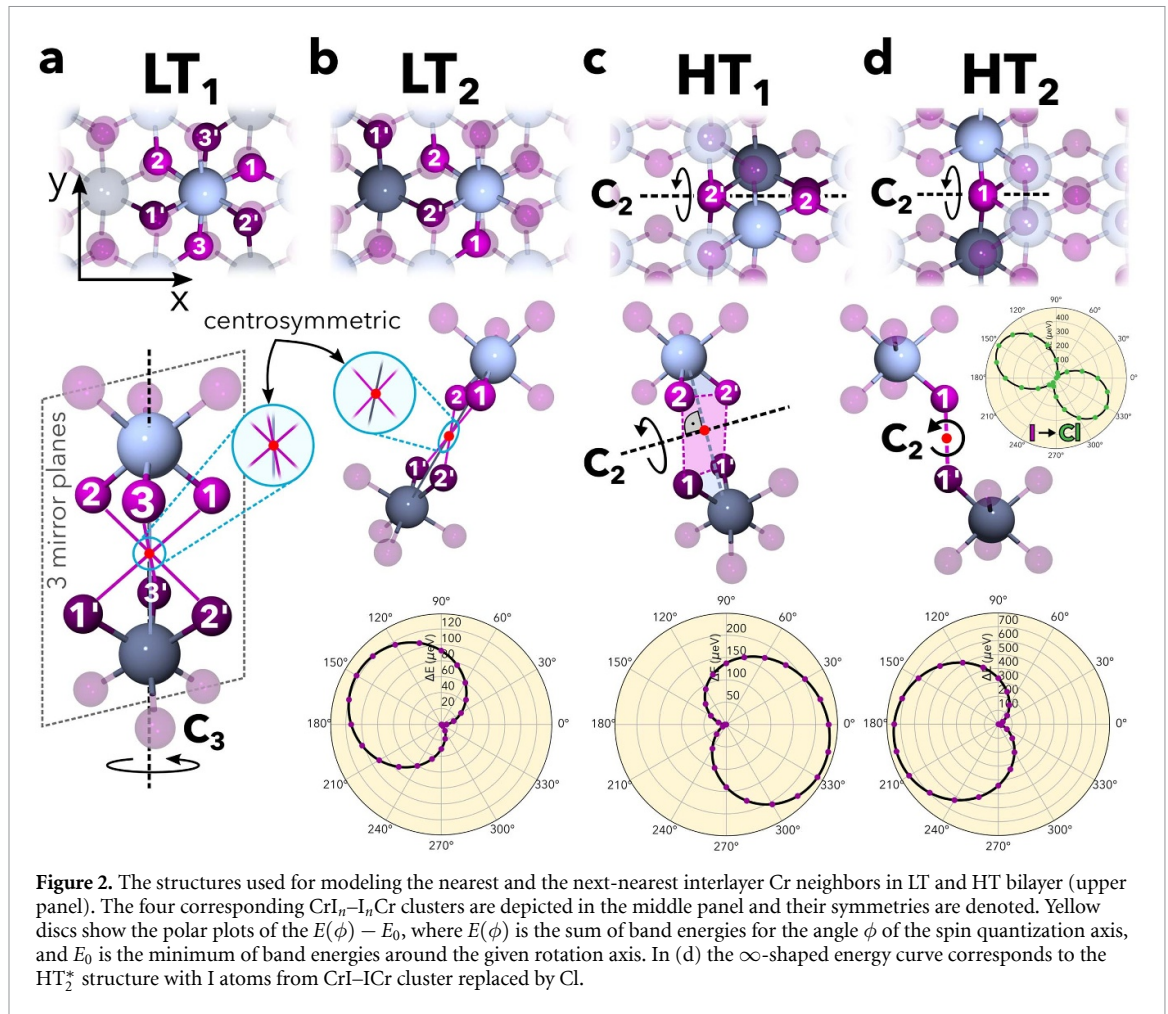
From equation (2), we define the SIA constant as $A = \Delta E_A / S^2$, where ΔE_A is the total variation of the SIA energy term $E_A(\phi)$ for the rotation of spin \mathbf{S} around a given axis. It can be easily derived that, for a fixed rotation axis, the energy $E_A(\phi)$ reaches extrema at $\phi_0^\pm = \arcsin\left(\frac{1}{2} \pm \frac{A_+}{2\sqrt{A_+^2 + 4A_-^2}}\right)^{1/2}$ and its total variation is $\Delta E_A = |E(\phi_0) - E(\phi_0 + \pi/2)|$. If spin rotates around the z -axis, the in-plane SIA constant A_{\parallel} is obtained, whereas if it rotates around the x - (or y -) axis the fit yields the out-of-plane SIA constant, A_{\perp} . Finally, if one performs the DFT calculations for the $\{\mathbf{S}_1 \parallel z \leftrightarrow \mathbf{S}_2 \circlearrowleft z\}$ and $\{\mathbf{S}_1 \parallel x \leftrightarrow \mathbf{S}_2 \circlearrowleft x\}$ sets of spin configurations, the \mathbf{D} , \mathbf{K} , A_{\perp} , and A_{\parallel} are obtained from fitting to equation (2). We discuss this below by applying the model to the two Cr spins from different layers.

2.3. Interlayer coupling of perpendicular Cr magnetic moments

Bilayer CrI_3 is an illustrative example as it reveals a few different scenarios of interlayer exchange coupling and elucidates the important role of the symmetry of local environment around Cr ions. We refer to the pair of Cr ions accompanied by surrounding ligands as ‘the $\text{CrI}_n\text{-I}_n\text{Cr}$ cluster’ (n is the number of ligands that participate in the exchange path between Cr ions). We consider the nearest and the next-nearest interlayer neighbors in both the LT and HT structures. In the chosen coordinate system the Cr–Cr bond lies along the x -axis and z -axis is perpendicular to the CrI_3 plane (see figure 2(a)). For each considered structure, we perform the symmetry analysis to double check whether the calculated off-diagonal \mathcal{J} -matrix elements comply with the extended Moriya rules exposed in supplementary information.

Starting with the LT bilayer, the nearest and the next-nearest interlayer Cr neighbors are modeled by LT_1 and LT_2 structures (see figures 2(a) and (b)). In LT_1 , the Cr–Cr bond displays inversion, threefold rotation axis parallel to the bond, and three vertical mirror planes. Therefore, the $\text{CrI}_3\text{-I}_3\text{Cr}$ cluster in LT_1 satisfies three Moriya rules (a, c, e) and consequently the exchange matrix must be diagonal. In complete agreement our calculations give all the zeros at the off-diagonal slots of the exchange matrix ($\mathcal{J}_{\text{LT}_1}$ in equation (S2)).

Moving further to the next-nearest neighbors, the $\text{CrI}_2\text{-I}_2\text{Cr}$ cluster in LT_2 has only the spatial-inversion



symmetry (Moriya rule a), constraining the $\mathcal{J}_{\text{LT}_2}$ to be symmetric and forbidding the DMI. On the other hand, no symmetry rule forbids the KI and our calculations reveal $K = 32 \mu\text{eV}$ (table 1). Here one can actually see the KI in action: with \mathbf{S}_1 fixed along the z -axis and \mathbf{S}_2 rotating around it, the energy of the system is changing according to the *cardioid* pattern which is a direct consequence of the KI (see the polar plot in figure 2(b)).

Moving the discussion to HT stacking, the x -axis is a twofold rotational axis for both the $\text{CrI}_2\text{-I}_2\text{Cr}$ in HT_1 and the $\text{CrI-I}\text{Cr}$ cluster in HT_2 structure (see figures 2(c) and (d)). Taking into account that the Cr-Cr bond is perpendicular to the x -axis, these two cases fall into the Moriya rule (d) category and the symmetry implies $J_{yx} = -J_{xy}$, $J_{zx} = -J_{xz}$, and $J_{zy} = J_{yz}$. Although KI is not forbidden by symmetry, our calculations reveal its total absence in HT_1 structure and a modest $K = 25 \mu\text{eV}$ in HT_2 .

Strikingly, both the nearest and the next-nearest interlayer neighbors in HT structure display considerable DMI in the range of 150–200 μeV (table 1). In Moriya's seminal paper it is shown that the DMI energy is linear in SOC [22]. Given that the SOC on

iodine (and not on chromium) gives the major contribution to MAE of monolayer CrI_3 [17, 21, 48], we assume that iodine's SOC is responsible as well for the interlayer DMI in bilayer CrI_3 . This assumption can be tested through ligand replacement. The SOC constant for valence electrons in solids scales as $\lambda \sim 1/Z^2$, where Z is the atomic number [49]. Therefore, by the rule of thumb, if iodines are replaced with chlorine the DMI would reduce $Z_{\text{I}}^2/Z_{\text{Cl}}^2 \approx 10$ times. This simple estimate works surprisingly well, as we reveal that the D is reduced 12 times when the two iodines in HT_2 cluster are replaced by chlorine (see figure 2(d) and table 1). Moreover, this example proves the local character of the interlayer DMI, showing that only the ligands in the vicinity of Cr-Cr pair play a role in mediating this anisotropic interaction. Otherwise, the DMI would not be reduced so drastically even after the iodines of the $\text{CrI-I}\text{Cr}$ cluster are swapped by chlorine because the other iodines are still present in the structure. The dependence of DMI on SOC is further discussed in section 2.5.

For the sake of completeness, we calculated the DMI between the third neighbors of HT structure using the 3×3 supercell (2×2 supercell is not

Table 1. The magnitude and the components of Dzyaloshinskii and Kitaev vectors. The last two columns present the out-of-plane and the in-plane SIA constants.

Structure [$\mu\text{eV} \rightarrow$]	$ \mathbf{D} $	D_x	D_y	D_z	$ \mathbf{K} $	K_x	K_y	K_z	A_{\perp}	A_{\parallel}
LT ₁ (figure 2(a))	0	0	0	0	0	0	0	0	253	0
LT ₂ (figure 2(b))	0	0	0	0	32	-14	24	-16	240	1
HT ₁ (figure 2(c))	175	0	50	-168	0	0	0	0	172	19
HT ₂ (figure 2(d))	166	0	-166	-4	25	-25	0	0	173	12
HT ₂ [*] (CrCl-ClCr)	14	0	-14	3	1	-1	0	0	163	186

sufficiently large for such calculations). The $D = 7 \mu\text{eV}$ is clearly dwarfed by those of the nearest and the next-nearest neighbors, providing an additional proof that the interlayer DMI in bilayer CrI₃ is short ranged, practically limited to the nearest neighbors.

To the best of our knowledge, the effect of stacking on SIA is not addressed in previous studies of bilayer or bulk CrI₃. Most often, it is assumed that the SIA obtained for monolayer persists in bilayer and bulk. However, SIA is a local property and as such is prone to changes of the environment of magnetic ion, e.g. by altering the stacking sequence. Remarkably, we obtained an increase of 50% in A_{\perp} from HT to LT stacking (table 1). Given that SIA largely contributes to magnetic anisotropy, one should take this change into account when estimating the critical temperature of bilayer or bulk CrI₃. Further, contrary to the LT bilayer which is isotropic to the in-plane spin rotations ($A_{\parallel} = 0$, like in the monolayer CrI₃ [27]), the HT bilayer is not, as our DFT calculations reveal a modest in-plane SIA of $A_{\parallel} \sim 10 - 20 \mu\text{eV}$. Therefore, the alternation of a stacking sequence can change SIA. Instructively, in HT bilayer the in-plane SIA is responsible for the distortion of the cardioid pattern presented in figure 2(c).

2.4. Interlayer coupling of perpendicular magnetizations

In this section we move further from the two-spin systems to provide the description of coupling between the perpendicular magnetizations of fully magnetized layers, where all the spins are pointing to the same direction. In general, when spins are randomly distributed, the total energy of $N \times N$ bilayer CrI₃ (that contains $2N^2$ spins per layer) is a sum of the nonmagnetic energy, the contributions from the *intralayer* and *interlayer* exchange coupling of spins, and SIA contributions at each spin site,

$$E_N = E_{N,\text{nm}} + \sum_{i_1, i_2=1}^{2N^2} \mathbf{S}_{i_1} \mathcal{J}_{i_1 i_2}^{\uparrow} \mathbf{S}_{i_2} + \sum_{l=1,2} \left[\frac{1}{2} \sum_{i_j, j_l=1}^{2N^2} \mathbf{S}_{i_l} \mathcal{J}_{i_l j_l}^{\leftrightarrow} \mathbf{S}_{j_l} + \sum_{i_l=1}^{2N^2} \mathbf{S}_{i_l} \mathcal{A} \mathbf{S}_{i_l} \right], \quad (5)$$

where $l = 1, 2$ is the layer index and i_l and j_l are indices numbering the spin sites. The *interlayer* exchange tensor $\mathcal{J}_{i_1 i_2}^{\uparrow}$ describes the coupling between the spins

i_1 and i_2 from different layers, whereas the *intralayer* exchange tensor $\mathcal{J}_{i_j j_l}^{\leftrightarrow}$ describes the coupling between spins i_j and j_l from the same layer l .

If we assume that all the spins from one layer point in the same direction, i.e. $\mathbf{S}_{i_l} \equiv \mathbf{S}_l$, the equation (5) greatly simplifies,

$$E = E_{\text{nm}} + \mathbf{S}_1 \left(\underbrace{\mathcal{J}_{A_1 A_2}^{\uparrow} + \mathcal{J}_{A_1 B_2}^{\uparrow} + \mathcal{J}_{B_1 A_2}^{\uparrow} + \mathcal{J}_{B_1 B_2}^{\uparrow}}_{\mathcal{J}^{\uparrow}} \right) \mathbf{S}_2 + \sum_l \mathbf{S}_l \left(\frac{1}{2} \mathcal{J}_A^{\leftrightarrow} + \frac{1}{2} \mathcal{J}_B^{\leftrightarrow} + 2\mathcal{A} \right) \mathbf{S}_l, \quad (6)$$

where $E = E_N/N^2$ and $E_{\text{nm}} = E_{N,\text{nm}}/N^2$ are the total and the non-magnetic energy expressed per unit cell. In equation (6) the contributions from A and B sublattices (see figures 1(a) and (b)) are separated so that $\mathcal{J}_{A_1 B_2}^{\uparrow}$ describes the interlayer coupling between all the spins at A_1 sites with all the spins at B_2 sites (N^2 of each). The tensor $\mathcal{J}_A^{\leftrightarrow}$ describes the interaction of a single spin at A site with all the other spins from the same layer. If we specify the spins $\mathbf{S}_1 = (0, 0, S_1)$ and $\mathbf{S}_2 = (S_2 \cos(\phi), S_2 \sin(\phi), 0)$ the equation (6) reads

$$E(\phi) = E_C + S_1 S_2 \left(\mathcal{J}_{zx}^{\uparrow} \cos(\phi) + \mathcal{J}_{zy}^{\uparrow} \sin(\phi) \right) + S_2^2 (Q_- \sin^2(\phi) + Q_+ \sin(2\phi)), \quad (7)$$

which is the same equation as equation (2). The parameters Q_- and Q_+ stemming from $\mathcal{J}^{\leftrightarrow}$ and \mathcal{A} will be used solely for fitting purposes and will not be further discussed, as our focus is on \mathcal{J}^{\uparrow} .

We calculated the off-diagonal elements of \mathcal{J}^{\uparrow} -matrix for HT bilayer and obtained a weak interlayer KI of $K = 18 \mu\text{eV}$. On the other hand, already from the spatial-inversion symmetry of HT bilayer we know that there is no DMI as the $A_1 A_2$ ($A_1 B_2$) contribution to the Dzyaloshinskii vector exactly cancels that from $B_1 B_2$ ($B_1 A_2$). Nevertheless, this does not mean that the interlayer DMI between the sublattices is zero. To inspect this, we modeled the $A_1 A_2$ sublattice of the HT structure by replacing the Cr atoms of the $B_1 B_2$ sublattice with Al (figure 3(a)) and obtained the Dzyaloshinskii vector with a magnitude of $D_{A_1 A_2} = 236 \mu\text{eV}$ per unit cell, or $5.55 \mu\text{eV} \text{ \AA}^{-2}$. Although the μeV scale does not seem promising, this is actually a remarkable result, as the estimated $\frac{D}{|J|}$ ratio is 80% (with J taken from [31]), much higher

than the 10% threshold considered promising for skyrmionics [50–52].

To the best of our knowledge there are no available measurements of interlayer DMI in 2D magnetic heterostructures, but there are in various three-dimensional multilayer stacks [41, 53–56]. In a TbFe/Pt/Co multilayer, the maximal effective DMI field obtained for Pt thickness of 1.2 nm is $B_{\text{DMI}} \approx 13 \text{ mT}$, which converted to the interfacial DMI energy yields $E_{\text{DMI}} \approx 44 \mu\text{J m}^{-2} = 2.75 \mu\text{eV \AA}^{-2}$ [41]. Compared to the $D_{A_1A_2}$ of HT bilayer, the DMI in TbFe/Pt/Co is twice weaker. The DMI energy recently measured in a variety of synthetic magnets made from Co, Pt, and Ir layers is even weaker than that, as it does not exceed $E_{\text{DMI}} \approx 11.3 \mu\text{J m}^{-2} = 0.71 \mu\text{eV \AA}^{-2}$ [55]. However, the demonstrations of purely electrical switching, i.e. the field-free control of magnetization by electrical currents [54–56], make these results particularly exciting as they open a possibility for designing vertical heterostructures with correlated magnetizations for logic applications [41]. We remark that the DMI in these metallic synthetic magnets is of Ruderman–Kittel–Kasuya–Yosida (RKKY) type [57], arising from spin-orbit scattering of conduction electrons by the atoms of the nonmagnetic layer (usually Pt or Ir), whereas in the semiconducting CrI_3 bilayer considered here the DMI is due to the iodine-mediated super-superexchange interaction between the magnetic moments localized on Cr atoms—the mechanism which is discussed in detail in section 2.5. Therefore, with increasing distance between the CrI_3 layers, the DMI is not expected to display the oscillatory behavior characteristic for RKKY interaction. Despite their different origin, the DMI hidden in bilayer CrI_3 is at least of comparable strength as the strongest known RKKY-type DMI in metallic three-dimensional magnets.

2.5. Dependence of DMI/KI on structural transformations and SOC

In this section we analyze in detail the DMI and KI between the sublattices of bilayer CrI_3 . We modeled the HT structure with the unit cell and replaced the Cr atoms on *B* sublattices with Al, as depicted in figure 3(a).

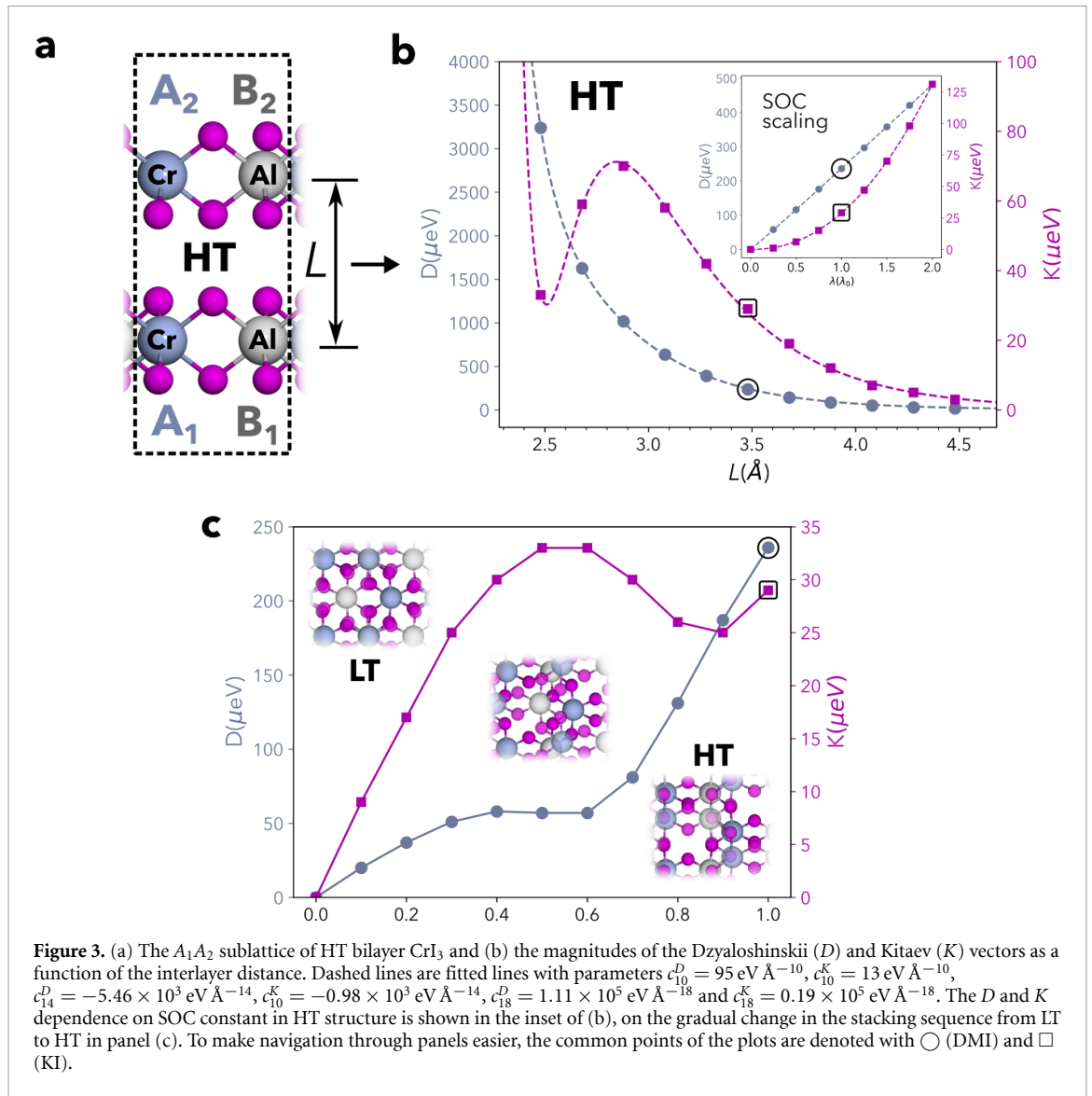
First, we inspected how these anisotropic interactions change as the interlayer distance L is varied. As shown in figure 3(b), the magnitude of both the DMI and KI display a fast, exponential-like decrease when L is larger than $\approx 3 \text{ \AA}$, consistently with the expected weak interaction between the layers across the VdW gap. At shorter separation, the evolution with L suggests a more complicated situation, especially for the KI which displays a non-monotonic behavior. Assuming a superexchange-like mechanism for both interactions, the dependence on the interlayer distance can be rationalized taking into account the possible exchange paths involving different transfer integrals (hopping terms) between Cr

and I ions and their expected dependence on the relative bond lengths l . One can identify three such hopping terms, corresponding to $d_{\text{Cr}}-d_{\text{Cr}}$ direct hopping ($t_1 \propto l^{-5}$), $d_{\text{Cr}}-p_{\text{I}}$ hopping ($t_2 \propto l^{-7/2}$) and $p_{\text{I}}-p_{\text{I}}$ hopping ($t_3 \propto l^{-2}$), where we adopted the bond-length dependence of Harrison [58]. In perturbation theory, the exchange interaction can be expressed quite generally as a sum of terms each with the form $t^n F(\lambda, U, \Delta)$, where $F(\lambda, U, \Delta)$ is a polynomial function of atomic SOC λ , charge transfer energy Δ , and on-site Coulomb interaction U and the exponent n depends on the number of hopping terms involved in the exchange path. For instance, the contribution to the exchange interaction arising from the direct $d-d$ hopping between Cr atoms scales as $t_1^2 \propto l^{-10} \sim L^{-10}$. Similarly, a Cr–I–Cr exchange path involving a single ligand $I-p$ intermediate state would scale as $t_2^4 \sim L^{-14}$, while a Cr–I–I–Cr exchange path would also include a $p-p$ transfer integral, scaling overall as $t_2^2 t_3^2 \sim L^{-18}$. Neglecting the details of the bond geometries and the angular dependence of each transfer integral and assuming that the dependence on the interlayer distance inherits the same scaling law of hopping terms, one can derive a general functional expression for both D and K that reads

$$I(L) = \frac{c_{10}^I}{L^{10}} + \frac{c_{14}^I}{L^{14}} + \frac{c_{18}^I}{L^{18}}, \quad (8)$$

where I stands for D or K and c_n^I are fitting parameters effectively including all the complicated dependence on interaction matrix elements. We stress the fact that different exchange paths can give rise to perturbation terms with the same scaling dependence on the interlayer distance, that are effectively regrouped in equation (8). As an example, the Cr–I–Cr exchange path shares the same L^{-14} dependence with a process where an electron is transferred from one Cr- d to the other magnetic atom through both ligands and then transferred back via a direct $d-d$ process.

Despite the underlying crude approximations, equation (8) captures surprisingly well the evolution of both DMI and KI as a function of the overall interlayer distance, as shown in figure 3(b). Remarkably, the non-monotonic dependence of KI can be quite naturally interpreted as arising from the competition of different super-superexchange processes occurring across the VdW gap. Notwithstanding the phenomenological nature of the fitting parameters, some general trends can be deduced. For both interaction terms, c_{14}^I is negative while c_{10}^I and c_{18}^I are positive: the largest coefficients are those involving $p-p$ hopping terms, which dominate at short separation, while in the opposite limit the first term—showing a slower decay—prevails. For instance, at the optimal distance $L_{\text{opt}} = 3.48 \text{ \AA}$, one has $D(L_{\text{opt}}) = (366 - 143 + 20) \mu\text{eV}$ and $K(L_{\text{opt}}) = (50 - 25 + 3) \mu\text{eV}$, with the dominant contribution arising from the slow-decaying $c_{10}^I L^{-10}$ term: a compression of 18% causes an increase of both interactions by more than 300%



and 140%, respectively, but the first two terms in equation (8) largely compensate each other and the third term starts to kick in, as $D(0.82L_{\text{opt}}) = (2.66 - 2.30 + 0.70) \text{ meV}$ and $K(0.82L_{\text{opt}}) = (0.36 - 0.41 + 0.12) \text{ meV}$.

It is worth reminding that the intralayer KI in monolayer CrI_3 (not to be confused with K as defined in section 2.2) has been shown to scale quadratically with ligand iodine SOC, the transition-metal SOC contribution being negligible [21]. The superexchange mechanisms leading to anisotropic exchange interactions are therefore different from those discussed in the seminal Moriya's paper [22], where it was assumed that the spin of the magnetic atom couples to its own orbital moment. On the other hand, the microscopic mechanisms at play are analogous to those analysed for related transition-metal dihalides, sharing with trihalides similar local bonding environments and strong magnetic anisotropies [59, 60]. To shed light on SOC dependence of interlayer anisotropic exchange couplings in bilayer CrI_3 , we varied the SOC constant from $\lambda = 0$ (no SOC) to

$\lambda = 2\lambda_0$ (double the original value), as shown in the inset of figure 3(b), and fitted the values to the power function $g(\lambda) = g_0\lambda^n$. The fit yielded $n_D = 1.03$ and $n_K = 2.19$ (see figure 3(c)), meaning that D is a linear function of λ whereas K has nearly quadratic behavior like that of the intralayer KI in monolayer CrI_3 . The scaling analysis on both SOC and interlayer distance suggests that superexchange mechanisms are effective in CrI_3 bilayer despite the presence of a VdW gap.

To examine the influence of a stacking sequence we gradually translated the upper layer along the \mathbf{a}_2 lattice vector, starting from the LT and ending with the HT structure (figure 3(c)). The different behavior of D and K with stacking alteration demonstrates the importance of angles in the Cr–I–I–Cr bonds for hopping processes that are governing the interlayer interaction. Along the inspected direction of translation, K reaches its maximum of $33 \mu\text{eV}$ on the halfway between the LT and HT, whereas the maximum of D of $236 \mu\text{eV}$ is in the HT structure. It is interesting to see that for structures that are intermediate between

LT and HT the DMI and KI are the same order of magnitude. Note that in order to find the global maximum of D and K one should inspect all possible translational directions, which is a demanding computational task that goes out of the scope of the present work.

3. Discussion

DFT calculations supported by Hamiltonian modeling reveal strong interlayer DMI in A_1A_2 (B_1B_2) sublattice of HT bilayer CrI_3 . At the microscopic scale, DMI in HT bilayer emerges between the nearest and the next-nearest interlayer Cr neighbors due to broken local spatial inversion. However, due to the global C_2 symmetry of sublattices, the contributions from A_1A_2 and B_1B_2 cancel each other resulting in zero net macroscopic DMI. In addition to DMI, there is an order of magnitude weaker interlayer KI that does not vanish due to symmetry. In LT structure there is no DMI as the Cr–Cr pair with their surrounding iodines are centrosymmetric. Despite the DMI in HT structure dies out at the macroscopic scale, the main result of this work is the demonstration of the ability of iodine ligands to efficiently mediate the anisotropic exchange between the magnetic layers. This ability comes from the strong SOC of spatially extended I-5*p* orbitals and is drastically reduced if iodine atoms are replaced by lighter ligands. The computational procedure developed in this work offers unprecedented accuracy in calculating the anisotropic exchange interactions. Being quite general, it can be applied to any magnetic material provided that the use of the magnetic force theorem is physically sound. In addition to the detailed analysis of the anisotropic interlayer exchange, we demonstrated that SIA heavily depends on stacking. Therefore, in estimating the Curie temperature of bilayer or bulk VdW magnet, one should not use the SIA calculated for a monolayer but instead should calculate the SIA for the particular system of interest.

With all being said, bilayer CrI_3 is not an appropriate 2D magnetic system for the experimental demonstration of interlayer DMI. Notwithstanding, we identified all the bricks needed to build one. Instead of attempting to modify the bilayer CrI_3 , the approach that seems more promising is to build from scratch a new heterostructure by finding an appropriate 2D magnet that can complement a layer of CrI_3 . Using a different 2D magnet as the second layer has a huge advantage for the interlayer DMI, as the spatial-inversion symmetry is trivially broken by different chemical composition of the two layers. To efficiently mediate the DMI between the magnetic ions, a candidate 2D magnet should have ligands that feature strong SOC. Most importantly, contrary to CrI_3 , it should have the in-plane magnetic anisotropy in order to maximize the $|\mathbf{M}_1 \times \mathbf{M}_2|$ product and its

MAE should be strong enough to compete with the interlayer Heisenberg exchange that would favor the (anti)parallel configuration of layers' magnetizations.

Within the CrX_3 family of 2D magnets only the CrCl_3 has an easy-plane MAE [27], but the other properties discredit it from potential candidacy. First, its MAE is very small and when combined with CrI_3 all the chances are that the interlayer Heisenberg exchange will prevail, redirecting the magnetization of CrCl_3 perpendicular to the plane. Second, the Cr–I–Cl–Cr interaction path is far less efficient than Cr–I–Cr in mediating DMI due to small SOC on Cl. We further note that due to the lattice constant mismatch between CrI_3 and CrCl_3 one would need to match 6×6 structure of CrI_3 with 7×7 structure of CrCl_3 to build a $\text{CrI}_3/\text{CrCl}_3$ heterostructure, ending up with 680 atoms in the supercell. Hence, due to high computational demands, we were not able to check these assumptions, thus leaving the search for a potential candidate for future studies.

4. Methods

DFT calculations are performed using the VASP code [61]. To describe the effects of electronic exchange and correlation we used the Perdew–Burke–Ernzerhof (PBE) functional [62]. Even though electron correlation beyond the PBE approximation may be expected to affect exchange interactions in VdW magnets [36, 37], it is currently debated whether a simplified, mean-field like correction including an effective Hubbard U on Cr-3*d* states in a DFT+ U scheme is appropriate for CrI_3 [35, 63–65]. As the I-5*p* bands provide an efficient screening of Coulomb interactions [18], we neglected the static mean-field Hubbard correction of DFT+ U , as recently suggested [65], and we adopted a plain PBE approach for our analysis. The lattice constant $a = 7.005 \text{ \AA}$ of monolayer CrI_3 is obtained from spin-polarized collinear DFT calculations assuming the FM ground state. The interlayer distance is set to $L_{\text{opt}} = 3.48 \text{ \AA}$, which corresponds to the experimental interlayer distance in bulk HT structure [29]. The bilayer made by stacking two monolayers was not relaxed any further. The lattice vector along the c -axis was set to 30 \AA so that the vacuum between periodic replicas along c -axis is 20 \AA thick. A cutoff of 450 eV is imposed onto the plane wave basis set and the total energies are converged to the precision of $10^{-9} \text{ eV/electron}$. We thoroughly tested the Brillouin zone sampling and in the end used a $8 \times 8 \times 1$ Γ -centered k -points mesh, meaning that the reciprocal cell of the 2×2 supercell was sampled with a $4 \times 4 \times 1$ k -points mesh. To sample the 3×3 supercell, needed to calculate the interaction between the third neighbors, we used the closest possible $3 \times 3 \times 1$ k -points mesh. The directions of magnetic moments on Cr atoms were constrained using the approach exposed in [43].

Data availability statement

All data that support the findings of this study are included within the article (and any supplementary files).

Acknowledgments

The authors acknowledge support from the Italian Ministry for Research and Education through PRIN-2017 Projects ‘TWEET: Towards ferroelectricity in two dimensions’ (IT-MIUR Grant No. 2017YCTB59), ‘Quantum 2D: Tuning and understanding Quantum phases in 2D materials’ (IT-MIUR Grant No. 2017Z8TS5B), and PRIN-2022 Project ‘SORBET: Spin-ORBit Effects in Two-dimensional magnets’ (IT-MIUR Grant No. PRIN 2022ZY8HJY). The computational resources were obtained from CINECA through the ISCRA initiative, in particular ISCRA-C Projects HP10CJ8MAY, HP10CUS5RM, and HP10CWPBNU. S S thanks Marko Milivojević for very useful discussions about the role of spin-orbit coupling in the superexchange interaction.

Author contributions


S P and S S conceived the project. S S performed the first-principles simulations and the model-Hamiltonian study, supported by P B. All the authors discussed the results and contributed to the writing of the manuscript.

Conflict of interest

The authors declare no competing financial or non-financial interests.

ORCID iDs

Srdjan Stavrić  <https://orcid.org/0000-0003-2097-0955>

Paolo Barone  <https://orcid.org/0000-0001-7222-8627>

References

- [1] Huang B et al 2017 Layer-dependent ferromagnetism in a van der Waals crystal down to the monolayer limit *Nature* **546** 270
- [2] Gong C et al 2017 Discovery of intrinsic ferromagnetism in two-dimensional van der Waals crystals *Nature* **546** 265
- [3] Klein D R et al 2018 Probing magnetism in 2D van der Waals crystalline insulators via electron tunneling *Science* **360** 1218
- [4] Song T et al 2018 Giant tunneling magnetoresistance in spin-filter van der Waals heterostructures *Science* **360** 1214
- [5] Wang Z, Gutiérrez-Lezama I, Ubrig N, Kroner M, Gibertini M, Taniguchi T, Watanabe K, Imamoğlu A, Giannini E and Morpurgo A F 2018 Very large tunneling magnetoresistance in layered magnetic semiconductor CrI₃ *Nat. Commun.* **9** 1
- [6] Gibertini M, Koperski M, Morpurgo A F and Novoselov K S 2019 Magnetic 2D materials and heterostructures *Nat. Nanotechnol.* **14** 408
- [7] Soriano D, Katsnelson M I and Fernández-Rossier J 2020 Magnetic two-dimensional chromium trihalides: a theoretical perspective *Nano Lett.* **20** 6225
- [8] Huang B et al 2018 Electrical control of 2D magnetism in bilayer CrI₃ *Nat. Nanotechnol.* **13** 544
- [9] Morell E S, León A, Miwa R H and Vargas P 2019 Control of magnetism in bilayer CrI₃ by an external electric field *2D Mater.* **6** 025020
- [10] Jiang P, Wang C, Chen D, Zhong Z, Yuan Z, Lu Z-Y and Ji W 2019 Stacking tunable interlayer magnetism in bilayer CrI₃ *Phys. Rev. B* **99** 144401
- [11] Song T et al 2019 Switching 2D magnetic states via pressure tuning of layer stacking *Nat. Mater.* **18** 1298
- [12] Xu Y et al 2022 Coexisting ferromagnetic–antiferromagnetic state in twisted bilayer CrI₃ *Nat. Nanotechnol.* **17** 143
- [13] Dolui K, Petrović M D, Zollner K, Plecháč P, Fabian J and Nikolić B K 2020 Proximity spin–orbit torque on a two-dimensional magnet within van der Waals heterostructure: current-driven antiferromagnet-to-ferromagnet reversible nonequilibrium phase transition in bilayer CrI₃ *Nano Lett.* **20** 2288–95
- [14] Zhang Y, Holder T, Ishizuka H, de Juan F, Nagaosa N, Felser C and Yan B 2019 Switchable magnetic bulk photovoltaic effect in the two-dimensional magnet CrI₃ *Nat. Commun.* **10** 1
- [15] Soriano D and Katsnelson M I 2020 Magnetic polaron and antiferromagnetic–ferromagnetic transition in doped bilayer CrI₃ *Phys. Rev. B* **101** 041402
- [16] Lei C, Chittari B L, Nomura K, Banerjee N, Jung J and MacDonald A H 2021 Magnetoelectric response of antiferromagnetic CrI₃ bilayers *Nano Lett.* **21** 1948
- [17] Lado J L and Fernández-Rossier J 2017 On the origin of magnetic anisotropy in two dimensional CrI₃ *2D Mater.* **4** 035002
- [18] Besbes O, Nikolaev S, Meskini N and Solovyev I 2019 Microscopic origin of ferromagnetism in the trihalides CrCl₃ and CrI₃ *Phys. Rev. B* **99** 104432
- [19] Kashin I V, Mazurenko V V, Katsnelson M I and Rudenko A N 2020 Orbital-resolved ferromagnetism of monolayer CrI₃ *2D Mater.* **7** 025036
- [20] Mermin N 1968 Crystalline order in two dimensions *Phys. Rev.* **176** 250
- [21] Xu C, Feng J, Xiang H and Bellaiche L 2018 Interplay between Kitaev interaction and single ion anisotropy in ferromagnetic CrI₃ and CrGeTe₃ monolayers *npj Comput. Mater.* **4** 1
- [22] Moriya T 1960 Anisotropic superexchange interaction and weak ferromagnetism *Phys. Rev.* **120** 91
- [23] Evans R F L, Rózsa L, Jenkins S and Atxitia U 2020 Temperature scaling of two-ion anisotropy in pure and mixed anisotropy systems *Phys. Rev. B* **102** 020412
- [24] Webster L and Yan J-A 2018 Strain-tunable magnetic anisotropy in monolayer CrCl₃, CrBr₃ and CrI₃ *Phys. Rev. B* **98** 144411
- [25] Lu X, Fei R and Yang L 2019 Curie temperature of emerging two-dimensional magnetic structures *Phys. Rev. B* **100** 205409
- [26] Xue F, Hou Y, Wang Z and Wu R 2019 Two-dimensional ferromagnetic van der Waals CrCl₃ monolayer with enhanced anisotropy and Curie temperature *Phys. Rev. B* **100** 224429
- [27] Lu X, Fei R, Zhu L and Yang L 2020 Meron-like topological spin defects in monolayer CrCl₃ *Nat. Commun.* **11** 1
- [28] Jaeschke-Ubiergo R, Suárez Morell E and Nunez A S 2021 Theory of magnetism in the van der Waals magnet CrI₃ *Phys. Rev. B* **103** 174410
- [29] McGuire M A, Dixit H, Cooper V R and Sales B C 2015 Coupling of crystal structure and magnetism in the layered, ferromagnetic insulator CrI₃ *Chem. Mater.* **27** 612
- [30] Sivadas N, Okamoto S, Xu X, Fennie C J and Xiao D 2018 Stacking-dependent magnetism in bilayer CrI₃ *Nano Lett.* **18** 7658

- [31] Jang S W, Jeong M Y, Yoon H, Ryee S and Han M J 2019 Microscopic understanding of magnetic interactions in bilayer CrI₃ *Phys. Rev. Mater.* **3** 031001
- [32] Soriano D, Cardoso C and Fernández-Rossier J 2019 Interplay between interlayer exchange and stacking in CrI₃ bilayers *Solid State Commun.* **299** 113662
- [33] Kong X, Yoon H, Han M J and Liang L 2021 Switching interlayer magnetic order in bilayer CrI₃ by stacking reversal *Nanoscale* **13** 16172
- [34] Li T et al 2019 Pressure-controlled interlayer magnetism in atomically thin CrI₃ *Nat. Mater.* **18** 1303
- [35] Ke L and Katsnelson M I 2021 Electron correlation effects on exchange interactions and spin excitations in 2D van der Waals materials *npj Comput. Mater.* **7** 1
- [36] Song K W and Fal'ko V I 2022 Superexchange and spin-orbit coupling in monolayer and bilayer chromium trihalides *Phys. Rev. B* **106** 245111
- [37] Song K W 2023 Interlayer superexchange in bilayer chromium trihalides *Phys. Rev. B* **107** 245133
- [38] Akram M, LaBollita H, Dey D, Kapaghian J, Erten O and Botana A S 2021 Moiré skyrmions and chiral magnetic phases in twisted CrX₃ (X = I, Br and Cl) bilayers *Nano Lett.* **21** 6633
- [39] Yang B, Li Y, Xiang H, Lin H and Huang B 2023 Moiré magnetic exchange interactions in twisted magnets *Nat. Comput. Sci.* **3** 314
- [40] Vedmedenko E Y, Riego P, Arregi J A and Berger A 2019 Interlayer Dzyaloshinskii–Moriya interactions *Phys. Rev. Lett.* **122** 257202
- [41] Avci C O, Lambert C-H, Sala G and Gambardella P 2021 Chiral coupling between magnetic layers with orthogonal magnetization *Phys. Rev. Lett.* **127** 167202
- [42] Xiang H, Lee C, Koo H-J, Gong X and Whangbo M-H 2012 Magnetic properties and energy-mapping analysis *Dalton Trans.* **42** 823
- [43] Ma P-W and Dudarev S L 2015 Constrained density functional for noncollinear magnetism *Phys. Rev. B* **91** 054420
- [44] Liechtenstein A I, Katsnelson M I, Antropov V P and Gubanov V A 1987 Local spin density functional approach to the theory of exchange interactions in ferromagnetic metals and alloys *J. Magn. Magn. Mater.* **67** 65
- [45] Solovyev I V 2021 Exchange interactions and magnetic force theorem *Phys. Rev. B* **103** 104428
- [46] Soriano D, Rudenko A N, Katsnelson M I and Rösner M 2021 Environmental screening and ligand-field effects to magnetism in CrI₃ monolayer *npj Comput. Mater.* **7** 1
- [47] Li X, Yu H, Lou F, Feng J, Whangbo M-H and Xiang H 2021 Spin Hamiltonians in magnets: theories and computations *Molecules* **26** 803
- [48] Kim J, Kim K-W, Kim B, Kang C-J, Shin D, Lee S-H, Min B-C and Park N 2020 Exploitable magnetic anisotropy of the two-dimensional magnet CrI₃ *Nano Lett.* **20** 929
- [49] Shanavas K V, Popović Z S and Satpathy S 2014 Theoretical model for Rashba spin-orbit interaction in *d* electrons *Phys. Rev. B* **90** 165108
- [50] Koshibae W and Nagaosa N 2014 Creation of skyrmions and antiskyrmions by local heating *Nat. Commun.* **5** 1
- [51] Zhang Y, Xu C, Chen P, Nahas Y, Prokhorenko S and Bellaiche L 2020 Emergence of skyrmionium in a two-dimensional CrGe(Se, Te)₃ Janus monolayer *Phys. Rev. B* **102** 241107
- [52] Xu C, Feng J, Prokhorenko S, Nahas Y, Xiang H and Bellaiche L 2020 Topological spin texture in Janus monolayers of the chromium trihalides Cr(I, X)₃ *Phys. Rev. B* **101** 060404
- [53] Han D-S et al 2019 Long-range chiral exchange interaction in synthetic antiferromagnets *Nat. Mater.* **18** 703
- [54] Wang K, Qian L, Ying S-C and Xiao G 2021 Spin-orbit torque switching of chiral magnetization across a synthetic antiferromagnet *Commun. Phys.* **4** 1
- [55] Kammerbauer F, Choi W-Y, Freimuth F, Lee K, Frömter R, Han D-S, Lavrijsen R, Swagten H J M, Mokrousov Y and Kläui M 2023 Controlling the interlayer Dzyaloshinskii–Moriya interaction by electrical currents *Nano Lett.* **23** 7070
- [56] Liang S, Chen R, Cui Q, Zhou Y, Pan F, Yang H and Song C 2023 Ruderman–Kittel–Kasuya–Yosida-type interlayer Dzyaloshinskii–Moriya interaction in synthetic magnets *Nano Lett.* **23** 8690
- [57] Fert A and Levy P M 1980 Role of anisotropic exchange interactions in determining the properties of spin-glasses *Phys. Rev. Lett.* **44** 1538
- [58] Harrison W A 1989 *Electronic Structure and the Properties of Solids* (Dover Publications)
- [59] Amoroso D, Barone P and Picozzi S 2020 Spontaneous skyrmionic lattice from anisotropic symmetric exchange in a Ni-halide monolayer *Nat. Commun.* **11** 5784
- [60] Riedl K, Amoroso D, Backes S, Razpopov A, Nguyen T P T, Yamauchi K, Barone P, Winter S M, Picozzi S and Valentí R 2022 Microscopic origin of magnetism in monolayer 3d transition metal dihalides *Phys. Rev. B* **106** 035156
- [61] Kresse G and Furthmüller J 1996 Efficient iterative schemes for *ab initio* total-energy calculations using a plane-wave basis set *Phys. Rev. B* **54** 11169
- [62] Perdew J, Burke K and Ernzerhof M 1996 Generalized gradient approximation made simple *Phys. Rev. Lett.* **77** 3865
- [63] Lee Y, Kotani T and Ke L 2020 Role of nonlocality in exchange correlation for magnetic two-dimensional van der Waals materials *Phys. Rev. B* **101** 241409
- [64] Sarkar S and Kratzer P 2021 Magnetic exchange interactions in bilayer CrX₃ (x = Cl, Br, and I): a critical assessment of the DFT + *U* approach *Phys. Rev. B* **103** 224421
- [65] Kvashnin Y O, Rudenko A N, Thunström P, Rösner M and Katsnelson M I 2022 Dynamical correlations in single-layer CrI₃ *Phys. Rev. B* **105** 205124